Original Article

Avicenna Journal of Medical Biotechnology
Volume 15, Issue 3, 139-156
https://doi.org/10.18502/ajmb.v15i3.12923

Application of Menstrual Blood Derived Stromal (stem) Cells Exert Greater Regenerative Potency Than Fibroblasts/Keratinocytes in Chronic Wounds of Diabetic Mice

Ebrahim Mirzadegan [1], Hannaneh Golshahi [1], Zahra Saffarian [1], Haleh Edalatkhah [1], Maryam Darzi [1], Somayeh Khorasani [1], Kioomars Saliminejad [2] and Somaieh Kazemnejad [1*]

1. Nanobiotechnology Research Center, Avicenna Research Institute, ACECR, Tehran, Iran
2. Reproductive Biotechnology Research Center, Avicenna Research Institute, ACECR, Tehran, Iran

*** Corresponding author:**
Somaieh Kazemnejad, Ph.D.
Nanobiotechnology Research Center, Avicenna Research Institute, ACECR, Tehran, Iran
Tel: +98 21 22432020
Fax: +98 21 22432021
E-mail: s.kazemnejad@avicenna.ac.ir
Received: 29 Aug 2022
Accepted: 15 Mar 2023

Abstract

Background: In this study we differentially showed the effects of cell-seeded bilayer scaffold wound dressing in accelerating healing process in diabetic ulcers that still remains as a major clinical challenge. The aim of the study was to compare immunomodulatory and angiogenic activity, and regenerative effect differences between Menstrual blood-derived Stem Cells (MenSCs) and foreskin-derived keratinocytes/fibroblasts.

Methods: The streptozotocin-induced diabetic mice model was developed in male C57/BL6 mice. A bilayer scaffold was fabricated by electrospining silk fibroin nanofibers on human Amniotic Membrane (AM). Dermal fibroblasts and keratinocyte isolated from neonatal foreskin and MenSCs were isolated from the menstrual blood of healthy women. The diabetic mice were randomly divided into three groups including no treatment group, fibroblast/keratinocyte-seeded bilayer scaffold group (bSC+FK), and MenSCs-seeded bilayer scaffold group. The healing of full-thickness excisional wounds evaluations in the diabetic mice model in each group were evaluated at 3, 7, and 14 days after treatment.

Results: The gross and histological data sets significantly showed wound healing promotion *via* re-epithelialization and wound contraction along with enhanced regeneration in MenSCs-seeded bilayer scaffold group with the most similarity to adjacent intact tissue. Immunofluorescence staining of mouse skin depicted a descending trend of type III collagen along with the higher expression of involucrin as keratinocyte marker in the MenSCs-seeded bilayer nanofibrous scaffold group in comparison with other treatment groups from day 7 to day 14. Moreover, higher levels of CD31 and von Willebrand factor (VWF), and also a higher ratio of M2/M1 macrophages in association with higher levels of the neural marker were observed in the bSC+MenSCs group in comparison with bSC+FK and no treatment groups.

Conclusion: Healing symptoms in wounds dressed with keratinocyte/fibroblast-seeded bilayer scaffold was significantly lower than MenSCs-seeded bilayer scaffold done on impaired diabetic wound chronicity.

Keywords: Bilayer scaffold, Diabetic wound, Fibroblasts, Keratinocyte, Menstrual blood stem cells

To cite this article: Mirzadegan E, Golshahi H, Saffarian Z, Edalatkhah H, Darzi M, Khorasani S, et al. Application of Menstrual Blood Derived Stromal (stem) Cells Exert Greater Regenerative Potency Than Fibroblasts/Keratinocytes in Chronic Wounds of Diabetic Mice. Avicenna J Med Biotech 2023;15(3):139-156.

Introduction

Worldwide increase in incidence of chronic non-healing diabetic wounds remain an ongoing challenge in advanced wound therapies. The prevalence of diabetes is increasing and expected to exceed 640 million people in 2040 [1]. Treatment of diabetic wounds face-complexity and poor healing outcomes that lead to more than half of diabetic wound cases that do not heal expressively. Hence, multidisciplinary approaches are

needed to treat these groups of patients [2].

Cell-loaded bioengineered skin graft substitutes open a new horizon in healing and regeneration of problematic wounds such as, large wounds, burns, pressure sores, diabetic ulcers, *etc* [3]. Three major components of a bioartificial skin including, Extra Cellular Matrix (ECM), cells and growth factors are responsible for dynamic wound closure and wound resolution. In normal wound healing process, a cross talk between fibroblast and keratinocyte modulate inflammatory stage toward synthesis and remodeling phase. Fibroblasts are the most populated stromal cells in dermis [4,5] and begin to migrate into the wounded area and proliferate to synthesize various ECM components such as collagen, elastin, laminin, fibronectin, and glycosaminoglycans [6]. Thus, the structural and mechanical integrity of sub-epithelial connective tissue is continuously maintained by fibroblasts. Furthermore, these cells have vital role in proliferation and migration of keratinocytes as well as modulation of the matrix metalloprotease activity based on a bilateral interplay with keratinocytes, which is critical during wound remodeling [7,8]. During closing of the wound defect, keratinocytes proliferate and migrate over underlying granulation tissue towards each other to close the wound and restore the physical barrier. In a reciprocal manner, keratinocytes stimulate fibroblasts to produce and secret growth factors which in paracrine response regulate epidermal keratinocyte proliferation and turnover [9]. Therefore, evaluation of fibroblast/keratinocyte-loaded bio-artificial skin grafts may provide new approach for regeneration of diabetic wound healing in comparison to mesenchymal-seeded bioengineered skin graft substitutes.

Furthermore, skin resident Mesenchymal Stem Cells (MSCs) are mainly located at the perivascular niche [10-14] and the granulation tissue at early stages after injury and become the most activated cells located in the granulation tissue. The MSCs proliferate and synthesize large amounts of the ECM, and upregulate growth factor expression which stimulates keratinocyte proliferation [15,16]. In fact, activated mesenchymal cells *via* epithelial-mesenchymal [17] and keratinocyte-fibroblast interactions [9] regulate skin homeostasis during wound healing process.

In a previous experiment we fabricated a bilayer skin substitute consisting of human Amniotic Membrane (AM) which was coated by an electrospun silk fibroin with its related *in vivo* biological behavior was approved [18]. In another study, we showed efficient wound healing using a synthetic nanofibrous bilayer skin substitute in a murine wound healing model [19]. As shown in very recent research, we demonstrated the superior capability of Menstrual blood Stem Cells (MenSCs)-seeded bilayer scaffold wound dressing to improve and accelerate the regenerative process in diabetic wound bed in comparison to bilayer scaffold alone, and AM as novel biologic wound dressings [20]. As an emerging concept, numerous investigations utilized MSCs from different sources due to their therapeutic properties including migratory, angiogenic, immunomodulatory and reparative potency [21-24]. Among mesenchymal stem cells, MenSCs have been preferred due to their important practical advantages such as availability, easy accessibility and lacking ethical problems.

The purpose of the present study was to reproduce our very recent experiment comparing commercial cell-based tissue engineered skin substitutes that are usually derived from human keratinocytes and fibroblasts supported by a scaffold of synthetic mesh or xenogeneic collagen. Accordingly, in this study we used neonatal foreskin-derived fibroblasts and keratinocytes seeded on bilayer scaffold composed of human AM and electrospun silk fibroin nanofibers [18,19] to treat full-thickness wounds in diabetic mice model in comparison to MenSCs seeded on the same scaffold wound dressing.

Materials and Methods

Ethics

This study was approved by bioethics committee of Avicenna Research Institute for all procedures and protocols (IR.ACECR.Avicenna.REC.1396.11). Forty-five ten-week-old male C57BL/6 mice weighing between 21-24 *g* were purchased from Pasteur Institute of Iran (Tehran, Iran). All animals utilized in this experiment, received humane care according to the Guide for the Care and Use of Laboratory Animals published by the National Institutes of Health [25]. Human placentas were obtained from healthy mothers with no-complicated term pregnancies after elective caesarean birth at Iran-Mehr Hospital (Tehran, Iran). All women provided written informed consent. Menstrual Blood (MB) samples were collected from healthy volunteer women who signed written informed consent for use of their samples and experiment data. Keratinocytes and fibroblasts were isolated from neonatal foreskin tissue harvested from circumcised healthy newborns aged 2-10 months. Each donor's parent signed an informed consent form and accepted by the Medical Ethics Committee of Avicenna Research Institute.

Isolation, cultivation, and characterization of MenSCs

MenSCs were isolated according to our protocol previously published [26]. Briefly, MB was collected at the second day of menstruation by a sterile Diva cup (Diva International Co, Lunette, Finland). The collected MB was resuspended in Phosphate Buffered Saline (PBS) supplemented with 2.5 *µg/ml* fungizone (Gibco, Scotland, UK), 100 *µg/ml* streptomycin, and 100 *U/ml* penicillin (Sigma-Aldrich, MO, USA), as well as 0.5 *mM* ethylenediamine tetraacetic acid (EDTA) (Merck). Mononuclear cells were isolated from MB suspension by Ficoll-Hypaque density-gradient centrifugation (GE-Healthcare) and washed in the supplemented PBS. The cells were cultured in complete DMEM-12 (Gibco,

Invitrogen, USA) supplemented with 10% Fetal Bovine Serum (FBS) (Gibco) and at 37°*C* in a humidified 5% CO_2 incubator. After subsequent expansion, MenSCs at passages 2-4 were characterized and cryopreserved for next experiments. Briefly, the test tubes containing 10^6 of the cultured cells in passages 2-4 were incubated individually with PE-conjugated monoclonal antibodies specific for CD29, CD45, CD73, CD105, and CD133 for 30 *min* at 4°*C*. Isotype-matched PE-conjugated antibodies were used as an isotype control. To evaluate OCT-4 expression, the cells were first fixed in 4% paraformaldehyde for 10 *min* and then washed. The cells were permeabilized with 0.1% saponin and washed and stained with rabbit anti-human OCT-4 antibody for 30 *min*, followed by 30 *min* incubation with FITC-goat anti-rabbit Ig (Avicenna Research Institute, Tehran, Iran). Considering the appropriate isotype controls, the cell populations were analyzed using a flow cytometer (Partec GmbH, Munster, Germany).

Isolation and cultivation of keratinocytes and fibroblasts

Isolation of keratinocytes and fibroblasts was performed according to protocols previously reported [27,28]. Briefly, the foreskins were transferred in the tube containing Hanks' Balanced Salt Solution (HBSS) supplemented with 2.5 *µg/ml* amphotericin B (fungizone), 100 *µg/ml* streptomycin, and 100 *U/ml* penicillin (Sigma). Each sample was washed immediately with PBS and then minced. The samples were placed in the tube containing (0.25% *v/v*) dispase (Gibco) in HBSS and incubated at 4°*C* overnight. Next day, the contents of each individual tube were decanted into a petri dish while dermal side faced down. The epidermis and dermis were separated from each other using narrow-tipped forceps. The epidermal layers were chopped into small pieces and 2.5 *ml* trypsin/EDTA (0.25% trypsin, 1 *mM* EDTA, Gibco) was added. The dishes were incubated at 37°*C* in a humidified 5% CO_2 incubator for 20 *min*, and finally to inactivate trypsin/EDTA, the dish contents were transferred into a tube containing 5 *ml* DMEM (Gibco) supplemented with 10% FBS and pipetted up and down. The suspension was passed through 70 *µm* mesh filter and then centrifuged at 200 *g* for 10 *min*. The resultant cell pellet was resuspended in Epilife medium (GIBCO Invitrogen, USA) and transferred into flasks coated by ECM protein. Primary keratinocytes were maintained at 37°*C* in a humidified 5% CO_2 incubator and the medium was changed next day. In parallel, for fibroblast isolation, the dermal layers were minced into small pieces, and followed by digestion with 0.05% collagenase A (Roche Applied Science, Penzberg, Germany) in DMEM with 10 *mg/ml* human serum albumin (Sigma-Aldrich, MO, USA) during overnight at 37°*C* with 5% CO_2. The suspension was then centrifuged at 400 *g* for 10 *min* and resuspended in Epilife medium. The primary fibroblasts were maintained at 37°*C* in a humidified 5% CO_2 incubator and cultivated by replacing the culture medium twice weekly. Finally, isolated fibroblasts and keratinocytes were utilized for experiments before the sixth passage.

Fabrication of wound dressings

The bilayer scaffold composed of silk fibroin and Human Amniotic Membrane (HAM) was fabricated according to our established protocol (Figure 1A) [19]. After fabrication, the circular bilayer scaffolds on the side of electro-spun silk fibroin were placed on round coverslips, put on the bottom of each well of 24-well cell culture plates and soaked with the complete culture medium for 30 *min*. After that, 150×10^3 MenSCs suspended in DMEM-F12 were transmitted. After keeping the plates in a humidified 5% CO_2 incubator at 37°*C* for 45 *min*, 200 *µl* of complete DMEM-F12 medium was transferred into the wells for two turns, each after 1 *hr* interval. Then, the plates were preserved in CO_2 incubator for overnight [20]. The seeding of fibroblast/keratinocyte on bilayer scaffold was performed similarly to what is mentioned above with minor difference. 50×10^3 fibroblasts suspension in DMEM-F12 were dropped on the bilayer scaffolds and kept in a humidified 5% CO_2 incubator at 37°*C* for 45 *min*. DMEM-F12 medium was added in two turns as alluded earlier and then the plates were incubated overnight. The next day after draining culture medium, 100×10^3 keratinocytes suspended in EpiLife medium were dropped on bilayer scaffolds and then the steps continued as described above (Figure 1B).

In vivo modelling

Forty-five male C57BL/6 mice were individually put in cages with controlled temperature (20±2°*C*) and humidity (50±10%). Pelleted diet (Behparvar Co, Iran) and water *ad libitum* were also administrated. Diabetes was induced according to our protocol [20] (Figure 1C). After confirmation of diabetes mellitus induction, animals were randomly allocated into three groups including: No-Treatment group (NT), fibroblast/keratinocyte-seeded bilayer scaffold treated group (bSC+FK), and MenSCs-seeded bilayer scaffold treated group (bSC+ MenSCs). Each group consisted of 15 mice and was equally divided into sub-groups according to the time points (3, 7, and 14 days after surgery).

Anesthesia was performed by intraperitoneal injection of 50 *mg/kg* ketamine (10% Ketamine, Alfasan Co., Woerden, Netherland) and 100 *µg/kg* medetomidine (Dorbene, syva, Spain). Full-thickness wounds were created by 5 *mm* biopsy punching (Kai Medical, Japan) on the back of mice seven days after induction of diabetes mellitus according to our protocol [20]. After hemostasis, the wound dressings were applied on the wound sites (Figure 1D, step 2). Circle washer splints were set to wound edges using EPIGLU ethyl-2-cyanoacrylate tissue adhesive (Meyer-Haake, Germany), and then the splints were fixed to the skin using 5-0 nylon (Teb Keyhan Inc, Iran) sutures (Figure 1D, steps 3 and 4). 3 *M* Tegaderm® film (Health Care,

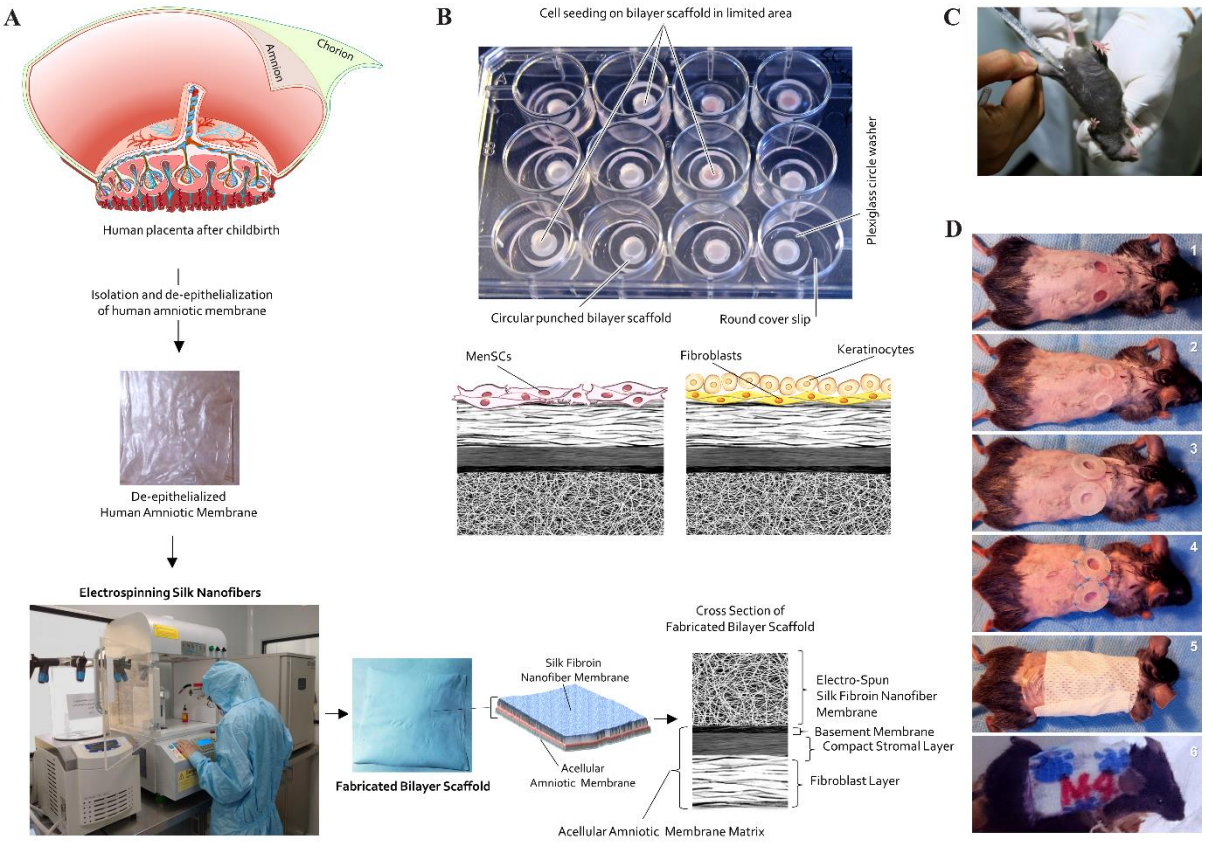

Figure 1. Steps of preparation and application of wound dressing in diabetic mice. A) Human placenta being surrounded by two layers of the amniotic membrane and chorion. The human amniotic membrane was separated from amniochorionic membrane, de-epithelialized and freeze-dried. Nanofibers were electro-spun on the basement membrane side of de-epithelized HAM by pumping silk fibroin solution by high voltage transmission. The schematic cross section of bilayer scaffold was showed. B) Cultivation of MenSCs and/or fibroblasts/keratinocytes for seeding on bilayer scaffold through sequential steps as mentioned in earlier report. C) Induction of diabetes by streptozotocin in C57BL/6 mice, D) Different parts of intervention (steps 1 to 6). 1) induction of full-thickness skin wounds, 2) wound dressing implantation, 3 and 4) splinting toward 5 and 6) wound dressing and bandage.

Germany) dressing and cohesive bandage (Pet Flex cohesive bandage, Andover, Netherland) were applied around the wounds (Figure 1D, steps 5 and 6). Atipamezole (500 *µg/kg*) (Alzane, syva, Spain) was injected in order to facilitate the recovery phase. Tramadol (10 *mg/kg*) (Caspian Tamin Co, Iran) and Enrofloxacin (15 *mg/kg*) (Nasr pharma, Iran) were subcutaneously administered for three consecutive days' post operation to increase the physiological recovery rate and relieve post-surgery pains.

Sample harvesting

At 3, 7, and 14 days post-surgery, complete wound area and approximately 2 *mm* of the margins of the wounds were punched [20]. For histopathological studies, samples were collected in Neutral-Buffered Formalin (NBF) 10%, and for immunofluorescence staining, samples were snap-frozen in OCT (Killik, Bio-Optica, Milan, Italy). Then, embedded frozen blocks were stored at -80°*C* until cryo-section operation. The specimens for RNA isolation were immediately frozen in liquid nitrogen and then stored at -80°*C*.

Gross examination and calculation of the healing progression

Skin wound healing was evaluated by photographic images at the time of wound induction and at 3, 7, and 14 days' post operation. Then, the Images were processed by ImageJ software (National Institutes of Health, Bethesda, MD). The percent of healing progression was calculated by following equation [29]:

% Healing progression=[[(WA0) - (OWAn + EWAn)]/(WA0)] ×100

(WA0): Wound area at the time of wound induction

(OWAn): Wound area at each time point consist of opening wound area

(EWAn): Epithelialized wound area at each time point

Histopathological evaluation

The Hematoxylin and Eosin (H&E) stained sections were evaluated by a veterinary anatomic pathologist. The dermal and epidermal heights of the healed and unwounded areas were also measured in H&E stained tissue sections at ×100 and ×400 magnifications, respectively.

Immunofluorescence staining assay

The diabetic wound samples were snap frozen and sectioned at a thickness of 7 μm and fixed in cold acetone, dry packed, and stored at -80°*C*. For evaluation of epidermal and dermal differentiation during wound healing, wound sections were incubated with anti-IVL, and anti-type III collagen, respectively as a primary rabbit polyclonal antibody, and then followed by an Alexa Fluor 488- donkey anti-rabbit IgG as a secondary antibody. The evaluation of angiogenic and neovasculogenic markers were performed by double immunofluorescence staining of the expression of CD31 and von Willebrand Factor (vWF) [30-34]. The wound sections were initially incubated with, anti-vWF antibody and then continued by Alexa Fluor 488-conjugated donkey anti-rabbit IgG antibody. Following, the staining process was completed by PE-conjugated rat anti mouse CD31. Cutaneous innervation was visualized through intracellular immunolabeling of the pan-neuronal marker protein gene product 9.5 (PGP9.5) by rabbit anti mouse PGP9.5. The PGP9.5 labeled sections were incubated with secondary antibody, Alexa Fluor 488-conjugated donkey anti-rabbit IgG.

For numeration of neutrophils and macrophages in diabetic wound bed, double immunofluorescence staining was designed. Hence, sections were incubated in cocktail of two antibodies, PE-conjugated anti-mouse Ly-6G antibody and Alexa Fluor 488-conjugated anti-mouse F4/80 antibody, respectively. Macrophage characterization according to M1 or M2 polarization was performed through two sets of double immunofluorescence staining; the first evaluation by Alexa Fluor 488-conjugated anti-mouse F4/80 antibody and PE-conjugated anti-mouse CD38 antibody for M1 phenotype, and the second evaluation by Alexa Fluor 488-conjugated anti-mouse F4/80 antibody and PE-conjugated anti-mouse CD206 for M2 phenotype [35]. In each evaluation, tissue nuclei were visualized with 4′6-diamidino-2-phenylindole (DAPI) (Sigma Chemical Company, St Louis, MO, USA). Five images were taken from the width of the wound at ×400 magnification after immunofluorescence staining. All images were individually analyzed using NIH ImageJ software as described in our previous report [20]. The antibody profile utilized for immunofluorescence staining in this study is mentioned in table 1.

Real-Time Quantitative Polymerase Chain Reaction (RT-qPCR)

Isolation of total RNA was carried out from diabetic wound area and a thin margin surrounded it by using AccuZol TM total RNA extraction solution (Bioneer, Korea) according to the manufacturer's instructions. Briefly, extracted total DNase-treated RNA (1 μg) was reverse transcribed into cDNA using random primers and thermocycler (Eppendorf, Germany). In next step, RT-qPCR analysis of gene expression was performed at Rotor-Gene Q System (Qiagen, CA) with the primers listed in table 2. All values were normalized

Table 1. Antibodies

Antibody	Fluorochrome	Isotype	Clonality/clone	Developer	Product code
Anti-human CD29	PE	Mouse IgG1, κ	M (MAR4)	BD Pharmingen	561795
Anti-human CD45	PE	Mouse IgG1, κ	M (HI30)	BD Pharmingen	560975
Anti-human CD73	PE	Mouse IgG1, κ	M (AD2)	BD Pharmingen	561014
Anti-human CD105	PE	Mouse IgG1	M (166707)	R&D systems	FAB10971P
Anti-Oct-4**	-	Rabbit IgG	P	Abcam	ab19857
Mouse IgG1, κ Isotype Control	FITC	Mouse IgG1, κ	M (MOPC-21)	BD Pharmingen	555748
Mouse IgG1, κ Isotype Control	PE	Mouse IgG1, κ	M (MOPC-21)	BD Pharmingen	551436
Anti-Collagen III*	-	Rabbit IgG	P	Abcam	ab7778
Anti-Involucrin*	-	Rabbit IgG	P	Abcam	ab53112
Anti-PGP9.5*	-	Rabbit IgG	P	Invitrogen	PA5-29012
Anti-mouse CD31	PE	Rat IgG2a, κ	M (390)	Biolegend	102408
Anti-Von Willebrand Factor*	-	Sheep IgG	P	Abcam	ab11713
Anti-mouse F4/80	Alexa Fluor®488	Rat IgG2a, κ	M (BM8)	Biolegend	123120
Anti-mouse CD38	PE	Rat IgG2a, κ	M (90)	Biolegend	102708
Anti-mouse CD206	PE	Rat IgG2a, κ	M (C068C2)	Biolegend	141706
Anti-mouse Ly-6G/Ly-6C (Gr-1)	PE	Rat IgG2b, κ	M (RB6-8C5)	Biolegend	108408
Anti-rabbit IgG (H+L) Antibody	Alexa Fluor®488	Donkey IgG	P	Invitrogen	A-21206
Rat IgG2a, κ Isotype control	Alexa Fluor®488	Rat IgG2a, κ	M (RTK2758)	Biolegend	400525
Rat IgG2a, κ Isotype control	PE	Rat IgG2a, κ	M (RTK2758)	Biolegend	400508
Rat IgG2b, κ Isotype control	PE	Rat IgG2b, κ	M (RTK4530)	Biolegend	400608
Anti-sheep IgG	-	Rabbit IgG	P	PADZA	pz86015

* This antibody has specific reactivity with mouse and some other species. P: Polyclonal; M: Monoclonal.
** This antibody has specific reactivity with Mouse, Sheep, Human, Rhesus monkey.

Table 2. Sequence of primers used in qRT-PCR

Gene product	Sense Primer Sequence (5'->3')	Antisense Primer Sequence (3'->5')	Size (base pairs)
Mmp9	CTCTCCTGGCTTTCGGCTG	TAGCGGTACAAGTATGCCTCTG	130
CXCL12/Cxcl12	AGTCAGCCTGAGCTACCGAT	CAGCCGTGCAACAATCTGAA	121
IDO1	CAGGCAGATGTTTAGCAATGA	GATGAAGAAGTGGGCTTTGC	91
Ptgs2	TACGACTTGCAGTGAGCGTC	AGCAAGGATTCGCTGTATGGC	189
Egr2	AGACAGAATCCCAGTAACTCTCAG	GTCAATGTAGATCATGCCATCTCC	169
B2M	CGAGATGTCTTGCTCCGTG	TCCATTCTCTGCTGGATGAGG	118
B2m	ACTGACCGGCCTGTATGCTA	AATGTGAGGCGGGTGGTAC	124

Mmp9: Matrix metallopeptidase 9; CXCL12: Chemokine (C-X-C motif) ligand 12; IDO1: Indoleamine 2,3-dioxygenase 1; Ptgs2: Prostaglandin-endoperoxide synthase 2; Egr2: Early growth response 2; B2m: Beta-2-microglobulin.

against beta-2-micro-globulin as housekeeping genes and expressed as fold change or relative expression using the 2-ΔΔCT formula [36]. Mean efficiencies and crossing point values for each gene were determined with LinReg PCR (version 11.0). The expression ratios of each bSC+MenSCs samples were calculated compared to other groups using relative expression software tool-2009 (REST-2009) (available at http://www.gene-quantification. info).

Statistical analysis

Results were presented as mean±standard error. Normally distribution of variables was evaluated by Kolmogorov-Smirnov normality test. Differences of means were analyzed by Two-way ANOVA, followed by Tukey's post-test used for analysis of multiple comparison groups. Probability value $p \leq 0.05$ was considered statistically significant.

Results

Identification of cell surface markers of MenSCs

Immunophenotypic analysis of surface markers revealed MenSCs are positive for CD29, CD73, and CD105 as MSCs markers and OCT-4 as an embryonic cell marker. However, they remain negative for hematopoietic stem cell markers such as CD45 and CD133.

Greater wound healing rate by application of bSC+MenSCs in comparison to bSC+FK

Gross evaluation showed that over time, an upward healing trend (of healing progress) was observed in all groups; however, this rate in bSC+MenSCs group was considerably greater than bSC+FK and NT groups at all-time points (Figures 2A and B).

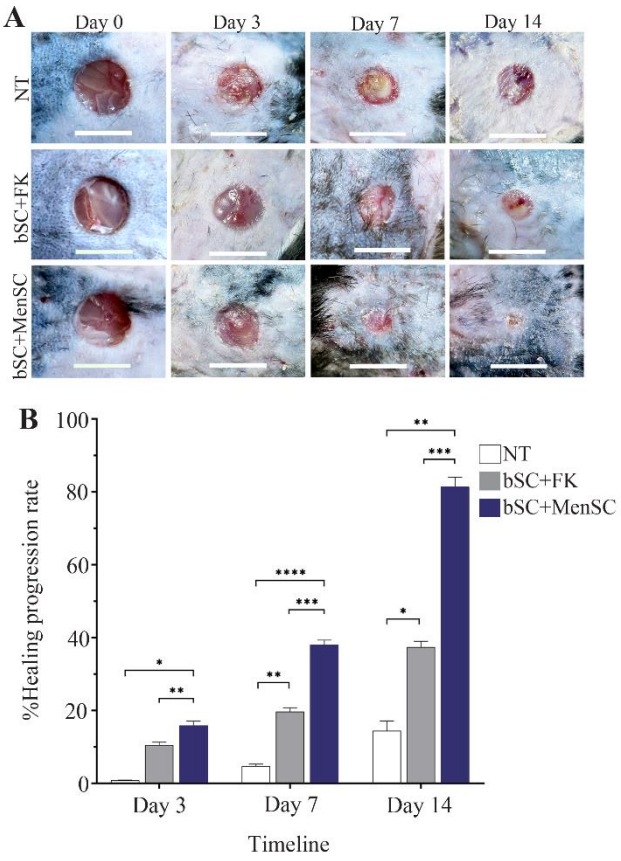

Figure 2. Gross evaluation of wound healing progression. A) Macro photographs of wounds from one selected mouse in each group in three time points. B) The percent of wound healing progression during three time points (p-values less than 0.05, 0.01, 0.001, and 0.0001 were shown with *, **, ***, and ****, respectively.

Application of bSC+MenSCs improve histopathological alterations more effectively than bSC+FK

As shown in figure 3A, three days after wound induction, in the NT group, full-thickness skin defects remained approximately unchanged and the wound surface was covered by crust and necrotic debris. The newly formed dermis was thin and mainly composed of immature granulation tissue with infiltration of neutrophils with diffuse pattern. Application of bSC+FK exhibited that the epithelialization was initiated from edges of the wounds and scab yet existed on wound surface. Below the scabs, a thin and immature granulation tissue with mild to moderate inflammatory cells infiltration was seen. Few disorganized collagen bundles were observed in newly formed dermis. Application of bSC+MenSCs as wound dressing caused observable re-epithelization beneath the crusts. The thickness of granulation tissue was greater than those of the bSC+FK group and the neovascularization was observed in the papillary layer.

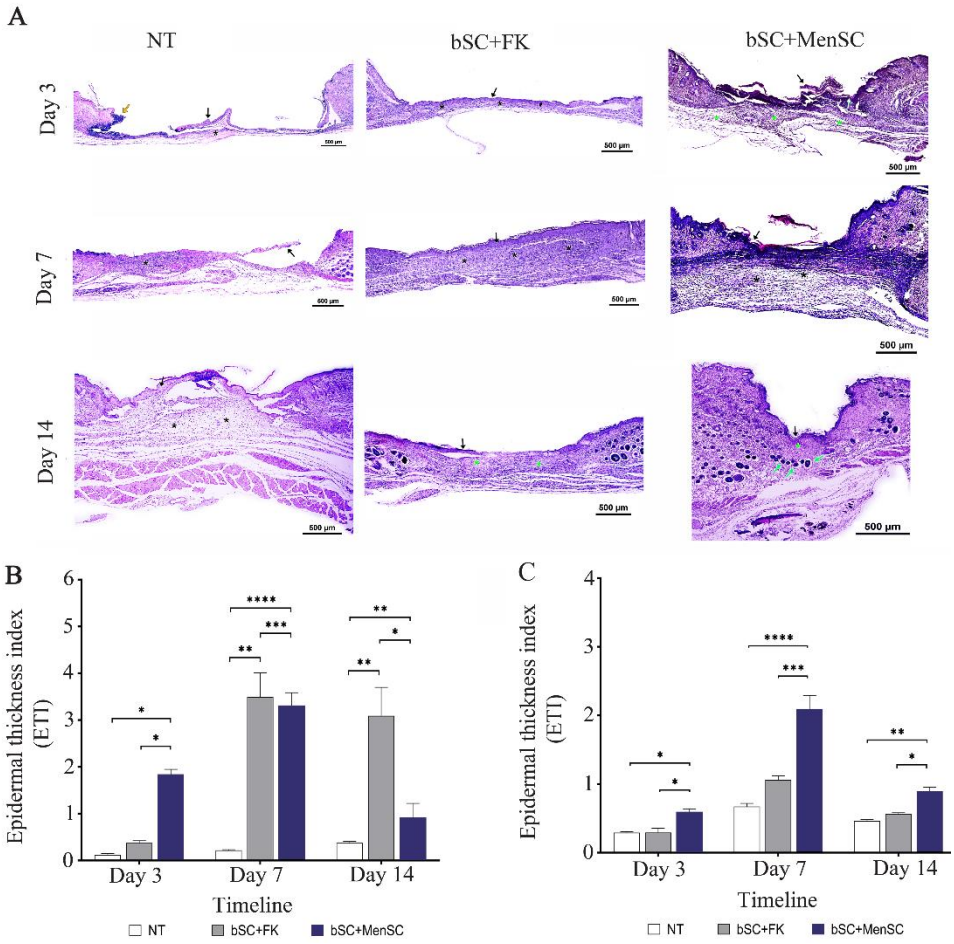

Figure 3. Microscopical evaluation of wound healing. A) H & E staining of healed wounds in different groups. Day 3: In NT group, lack of epidermal regeneration (black arrow), scab formation (red arrow) and thin granulation tissue in dermis (black star), are noted. In bSC+FK group, denuded wound covered by fibrino necrotic exudate (black arrow) in the central part and inflammatory cell infiltrations (black star) in newly-formed dermis is noticeable. In bSC+MenSCs group, sign of regeneration (white arrow) specially in wound borders beneath the remnant of wound dressing (black arrow) is detected. Also note the immature and edematous granulation tissue (green star) in dermis. Day 7: in NT group, the epidermal regeneration is not complete (black arrow) and also note to hyper cellular granulation tissue in dermis mainly occupied with inflammatory cells (black star). In bSC+FK group, note to regenerated hyperplastic and stratified epidermis (black arrow) and proliferating granulation tissue (black star). In bSC+MenSCs group, the re-epithelization is almost acceptable (black arrow) and in dermis a hyper cellular and edematous granulation tissue (black star) with noticeable vascular density is observed. Day 14: in NT group the newly formed epidermis was characterized by immature keratinocytes (black arrow) and new dermis was considered by an immature granulation tissue (black star). In bSC+FK group, the re-epithelization is not complete specially in central part (black arrow) and in dermi, note to hyper cellular granulation tissue (green arrow). In bSC+ MenSCs group, more mature stratified squamous epithelium (black arrow), dense collagenous bundles (green star) and well-recovered skin appendages (green arrow) are noted. B and C) The averaged Dermal Thickness Index (DTI) and Epidermal Thickness Index (ETI), respectively. p-values less than 0.05, 0.01, 0.001, and 0.0001 were shown with *, **, ***, and ****, respectively.

In NT group, seven days after wound induction, the defect was not filled completely, yet. The dermis was composed of immature granulation tissue and collagen fibrils arranged in a haphazard form in dermis. Application of fibroblast/keratinocyte-seeded on bilayer scaffold caused regenerated hyperplastic epidermis covering the wound surface. In sub epidermal layer, a highly vascularized and proliferating granulation tissue, consisting of more active fibroblasts, mild to moderate infiltration of inflammatory cells with slight superficial edema were detected. The connective tissue bundles were loosely arranged in the newly formed dermis. Using MenSCs-seeded bilayer scaffold initiated observable regeneration in both epidermal and dermal sites. The dermis was occupied with relatively mature granulation tissue and collagen bundles were arranged more regularly showing that dermal regeneration is boosted using MenSCs. Blood vessel density was noticeable in dermis. However, there were no signs of hair follicles or other adnexa formation in the regenerated dermis at this time point.

On day 14 after wound induction, cases belonging to the NT group demonstrated partial re-epithelization. Fibroblasts proliferation and mild to moderated infiltra-

tion of inflammatory cells in dermis were also seen. However, the wound sites were devoid of the skin adnexa. Histological examination of wounds in group applied by fibroblast/keratinocyte-seeded on bilayer scaffold 14 days after grafting revealed approximately well-recovered epidermal layers with more mature differentiation. The wound bed was mainly filled with fibroblast proliferation. Collagen bundles were arranged nearly parallel to the epidermis in the regenerated dermis. The inflammatory reaction was mild. Granulation tissue displayed reduction in the number of vessels mainly in the deeper layers of the wound. Histopathological evaluation showed that after application of MenSCs-seeded bilayer scaffold on wound site reasonably noticeable re-epithelization occurred. The new dermis was composed of relatively mature connective tissue and in some cases, well-recovered skin appendages were detected. The amount of inflammatory reaction was significantly scant (Figure 3A).

The mean Epidermal Thickness Index (ETI) was calculated at three time points for each study groups. The mean ETI of bSC+MenSCs group at day 3 was significantly higher than NT ($p<0.05$) and bSC+FK ($p<0.05$). Interestingly, a significant reduction of epidermal thickness to the optimal level was observed in bSC+MenSCs group from day 7 to 14 and at day 14, the epidermal thickness of this group was near to the thickness of adjacent epidermis. However, epidermal thickness in NT group was still measured at the lowest level (Figure 3B). The mean DTI of bSC+MenSCs group calculated at day 3 was significantly higher than NT ($p<0.05$) and bSC+FK ($p<0.05$), and at day 7 was also significantly higher than NT ($p<0.0001$) and bSC+FK ($p<0.001$). At the last time point (day 14), the measured mean DTI of bSC+MenSCs group showed that scar thickness considerably was restored to the optimal level (DTI ≤1). However, the dermal thickness in other groups was lower that native adjacent dermis (Figure 3C).

Identifying keratinocyte maturation in diabetic wounds dressed by the cell-seeded bilayer scaffolds

Normal differentiation during wound healing is characterized by restoration of expression of differentiation markers like Involucrin (IVL) in the neo-epidermis. Our data determined the higher expression of IVL by application of the cell-seeded bilayer scaffold in stimulation of diabetic wounds at day 7 and 14 in comparison to NT group. However, the IVL immunoreaction in bSC+MenSCs group was considerably higher than bSC+FK group and NT group at days 7 and 14 (Figures 4A and B).

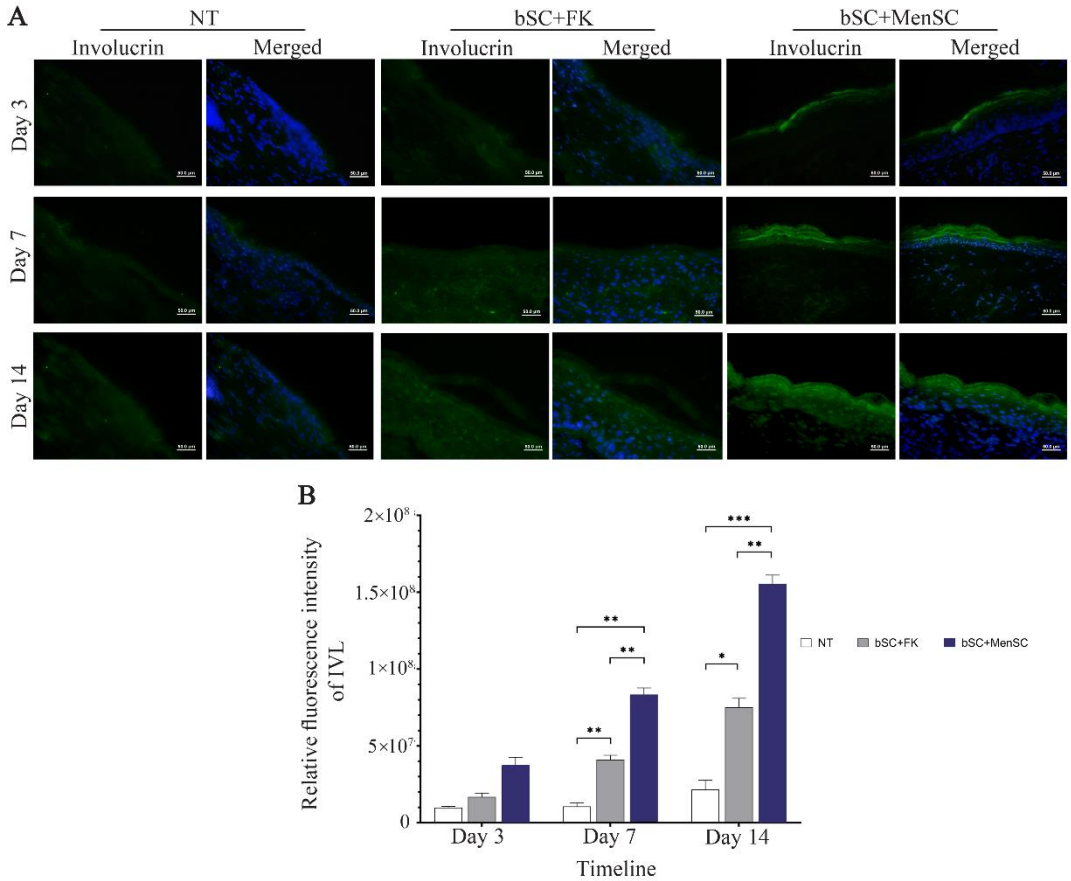

Figure 4. Evaluation of IVL expressions in the study groups. A) IVL expression in diabetic wounds was visualized by immunofluorescence staining through Alexa Fluor®488 labeling of IVL. These sections were also counterstained with DAPI. Scale bar = 50 μm. B) Relative fluorescence intensity of IVL expression of diabetic wounds was compared in different groups. p-values less than 0.05, 0.01, 0.001, and 0.0001 were shown with *, **, ***, and ****, respectively.

Identifying type III collagen expression in diabetic wounds dressed by the cell-seeded bilayer scaffolds

In NT and bSC+FK groups, increasing expression of type III collagen was significantly determined from day 3 to day 14. However, in bSC+MenSCs group the expression pattern of collagen III demonstrated an upward trend from days 3 to 7 and then a downward trend from days 7 to 14 (Figures 5A and B).

Enumeration of inflammatory cells infiltration in diabetic wounds dressed by the cell-seeded bilayer scaffolds

In NT group, significant infiltration of neutrophils in wound site was noticed in all time points. However, conspicuous decline of neutrophilic infiltration in diabetic wound dressed by MenSCs-seeded bilayer scaffold occurred at day 14 and the reduction was more significant by application of bSC+MenSCs in comparison to NT group ($p<0.001$) and bSC+FK ($p<0.05$). The evaluation of macrophages showed that an increase in the count of macrophages in all groups occurred over time, but the total number of macrophages in treated groups was not remarkably different at each three time points. The total number of macrophages in NT group was significantly higher in comparison with diabetic wound dressed by MenSCs-seeded bilayer scaffold at day 14 ($p<0.0001$) (Figures 6A and B).

Furthermore, from day 3 to day 14, an increasing number of $F4/80^{+}CD38^{+}$ phenotype (M1 macrophage) was detected in NT and bSC+FK groups and at day 7, the mean cell count of $F4/80^{+}CD38^{+}$ phenotype in bSC+MenSCs group showed statistically significant expansion in comparison with NT group ($p<0.01$) and bSC+FK group ($p<0.01$). Remarkable reduction was determined in the mean cell count of $F4/80^{+}CD38^{+}$ phenotype in bSC+MenSCs group at day 14 compared to the NT and bSC+FK groups ($p<0.05$ and $p<0.05$, respectively) (Figures 7A and C).

While, there were no significant differences in the mean cell count of $F4/80^{+}CD206^{+}$ (M2 macrophage) phenotype among the different groups at day 3, the low frequency of $F4/80^{+}CD206^{+}$ phenotype was observed in NT and bSC+FK groups at day 7 and day 14. Interestingly, we determined a considerable increase in $F4/80^{+}CD206^{+}$ phenotype in the diabetic wound dressed by MenSCs-seeded bilayer scaffold comparing NT

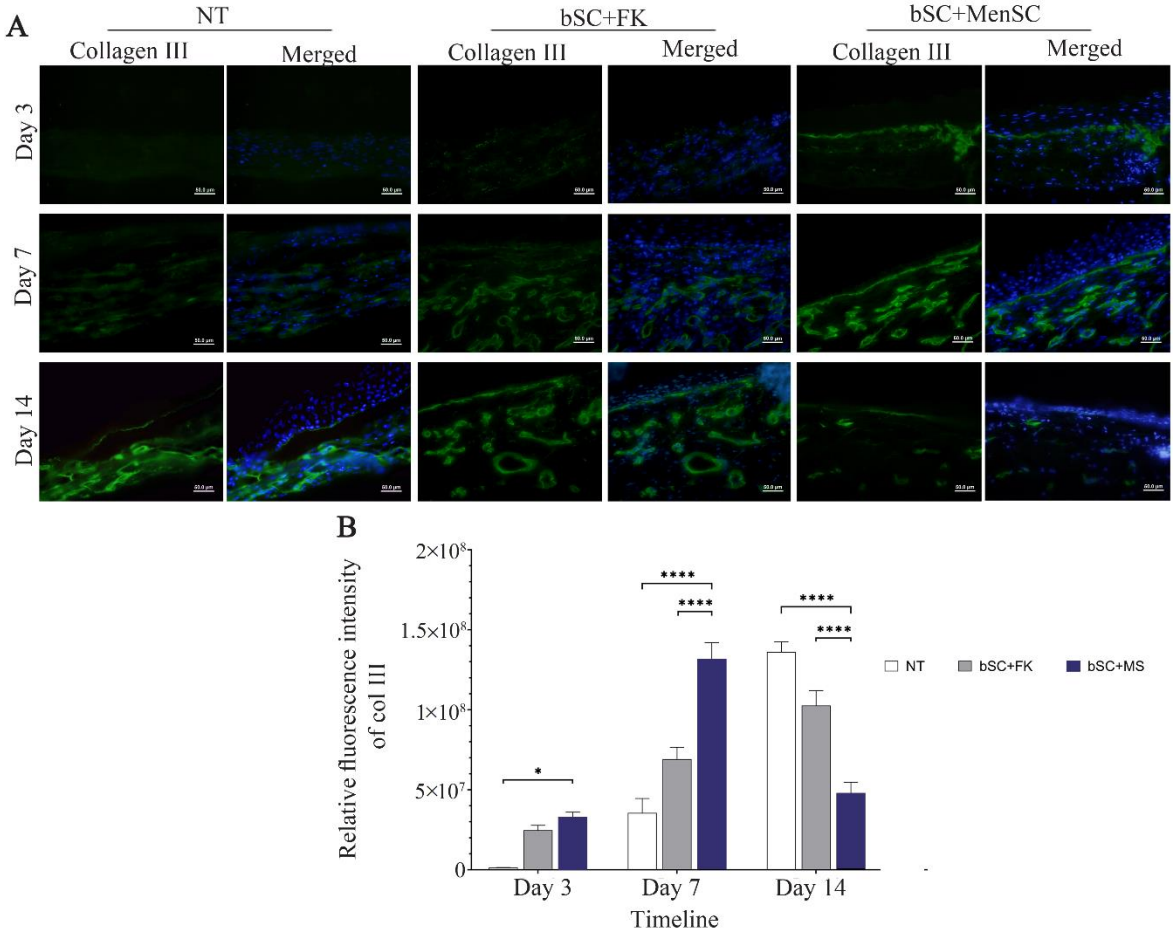

Figure 5. Evaluation of Type III collagen expressions in the study groups. A) Type III collagen levels in diabetic wounds was visualized by immunofluorescence staining through Alexa Fluor®488 labeling of Type III collagen. These sections were also counterstained with DAPI. Scale bar = 50 μm. B) Relative fluorescence intensity of type III collagen expression of diabetic wound. p-values less than 0.05, 0.01, 0.001, and 0.0001 were shown with *, **, ***, and ****, respectively.

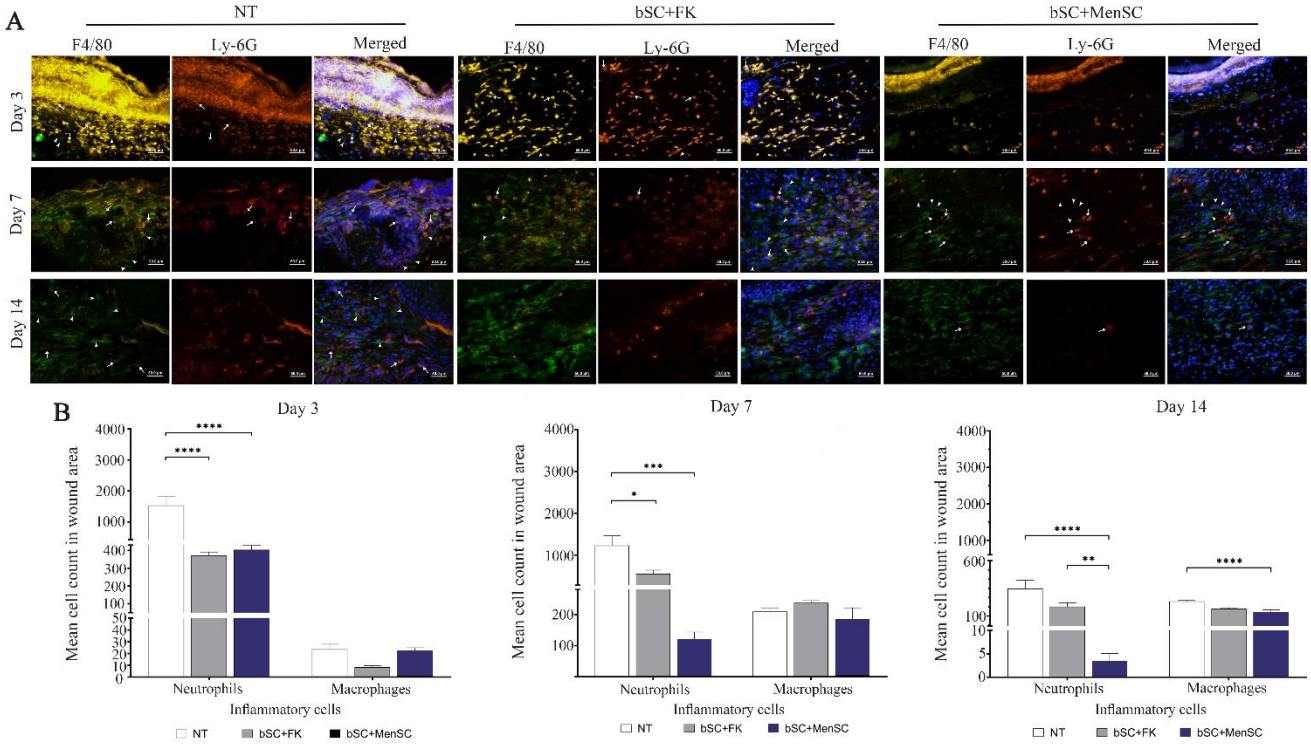

Figure 6. Neutrophil and macrophage enumerations in diabetic wound area. A) Neutrophil and macrophage were labeled by double immunofluorescence staining of diabetic wound sections by PE conjugated anti-Ly-6G/Ly-6C (Gr-1) targeted neutrophils (white arrows) and Alexa Fluor®488 conjugated anti-F4/80 targeted macrophages (white arrowhead). These sections were also counterstained with DAPI. Scale bar = 50 μm. B) Quantitative analysis of inflammatory cell enumerations at three time points among all groups. p-values less than 0.05, 0.01, 0.001, and 0.0001 were shown with *, **, ***, and ****, respectively.

group and bSC+FK ($p<0.0001$ and $p<0.0001$ respectively) at day 7, and day 14 (Figures 7B and D).

The effect of cell-seeded bilayer scaffold wound dressings on neovasculogenesis and angiogenesis

CD31 expression pattern exhibited statistically significant increase in bSC+FK group in comparison to NT group at day 7 ($p<0.0001$) and day 14 ($p<0.0001$), respectively. However, the expression of CD31 and especially vWF in bSC+MenSCs group were considerably higher in comparison to other groups at three time points (Figures 8A-C).

The effect of cell-seeded bilayer scaffold wound dressings on innervation in diabetic wound healing

The PGP9.5 expression in diabetic wound sections was assessed through relative fluorescence intensity measurement of PGP9.5 immunofluorescence patterns. The PGP9.5 assessment of diabetic wound area represented statistically significant increase in bSC+MenSCs group in comparison to other groups at day 7 and day 14 (Figures 9A and B).

Differential transcription pattern of wound healing related genes in different wound dressing

During wound healing in diabetic mice, the gene expression of some critical Inflammatory, immunomodulatory and angiogenic biomarkers were analyzed. *IDO1* and *Ptgs2* are implicated in immunomodulation and inflammation, respectively. There was also noteworthy increase in *IDO1* expression ratio in bSC+MenSCs in comparison to NT and bSC+FK groups at three time points. On the other hand, bSC+MenSCs group displayed descending trend *Ptgs2* expression in comparison to NT group and bSC+FK group at three time points. *Egr2*, the gene involved in M2 macrophage polarization showed statistically significant increase compared to NT group and bSC+FK group at day 3, day 7 and day 14.

Application of MenSCs-seeded bilayer scaffold on diabetic wound bed caused higher expression of *CXCL12* in comparison to the NT group at three time points. Lower level of *CXCL12* expression in bSC+MenSCs group in comparison to bSC+FK group was observed at days 3 and 7, However, significant expression occurred at day 14. Significant superiority of *Mmp9* gene expression was identified in bSC+MenSCs group in comparison to NT group at day 3 and bSC+FK group at all-time points. Furthermore, upregulation of Vascular Endothelial Growth Factor A (VEGFA) mRNA level was sharper in MenSCs-seeded bilayer scaffold compared to NT group, and bSC+FK group at three time points (Figure 10).

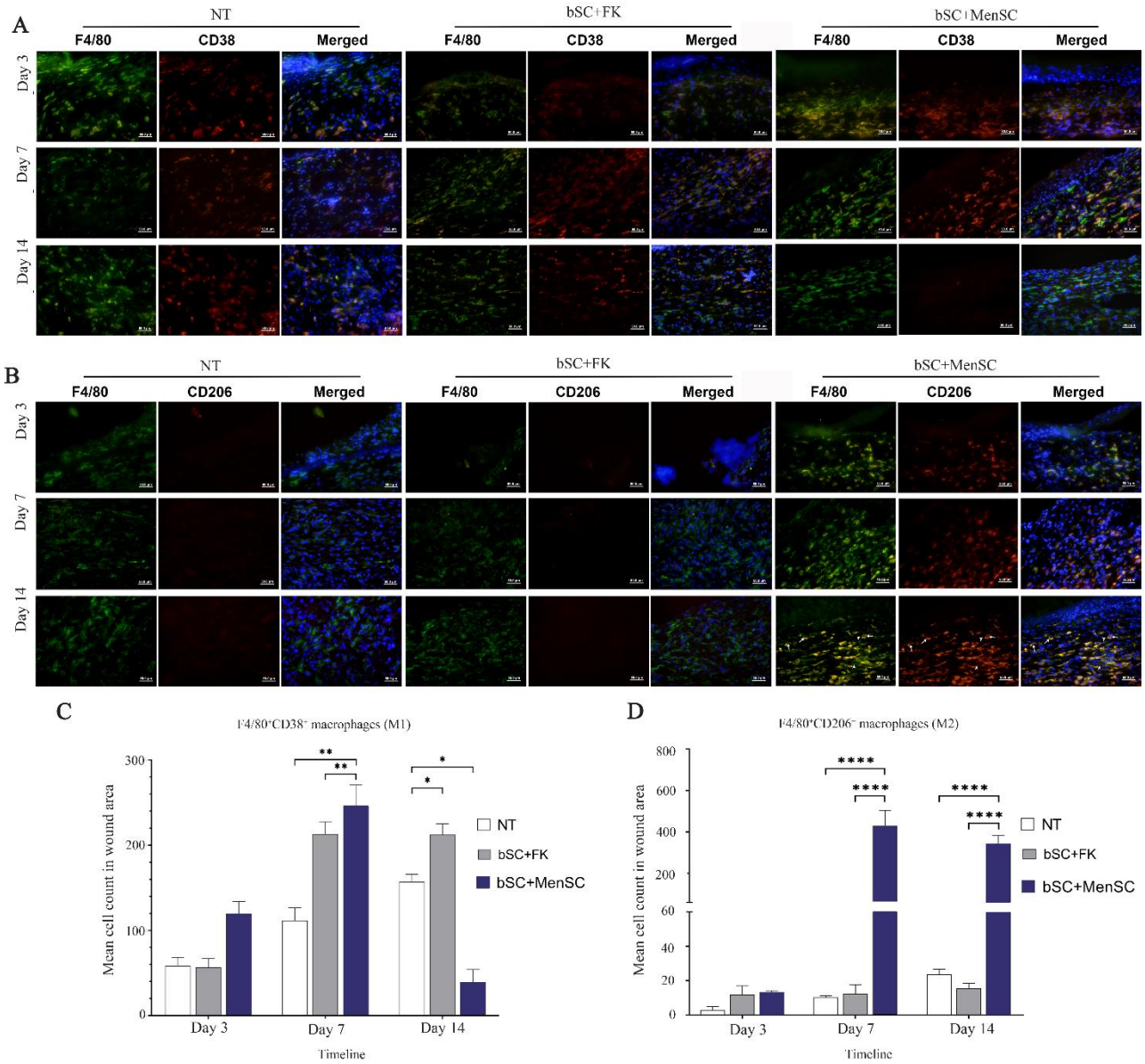

Figure 7. Effect of diabetic wound dressing on M1 and M2 macrophage subpopulations. A) M1 macrophages were labeled by double immunofluorescence staining of diabetic wound sections for Alexa Fluor®488 conjugated anti-F4/80 and PE conjugated anti-CD38. B) M2 macrophages were labeled by double immunofluorescence staining of diabetic wound sections through Alexa Fluor®488 conjugated anti-F4/80 and PE conjugated anti-CD206. Nuclei were visualized with DAPI (scale bar = 50 μm). C) Comparative evaluation of M1 phenotype subpopulation in diabetic wound treated in study groups. D) Comparative evaluation of M2 phenotype subpopulation in diabetic wound treated in study groups. p-values less than 0.05, 0.01, 0.001, and 0.0001 were shown with *, **, ***, and ****, respectively.

Discussion

In the present study for the first-time, we applied bilayer scaffold composed of AM and silk fibroin loaded with fibroblast/keratinocyte for healing of the diabetic wound in comparison to what is known as enhanced regenerative properties of MenSCs integrated in bilayer scaffold. There are several reports that indicate that keratinocyte and fibroblast interactions have central role in the wound healing and fibroblast differentiation potentially affects epithelial wound closure and scar remodeling [9]. However, in impaired diabetic wound, healing progression was significantly higher when MenSCs-seeded bilayer scaffold wound dressing was used in comparison to the fibroblast/keratinocyte-seeded bilayer wound dressing. Pertaining to epithelialization as an essential phase of the wound healing process, expression of IVL was assessed as a marker of migrating differentiated keratinocytes. As mentioned before, IVL expression was determined significantly higher in bSC+FK group in comparison to NT group at day 7 and day 14 and probably related to the reported properties of keratinocytes-seeded on bilayer scaffold

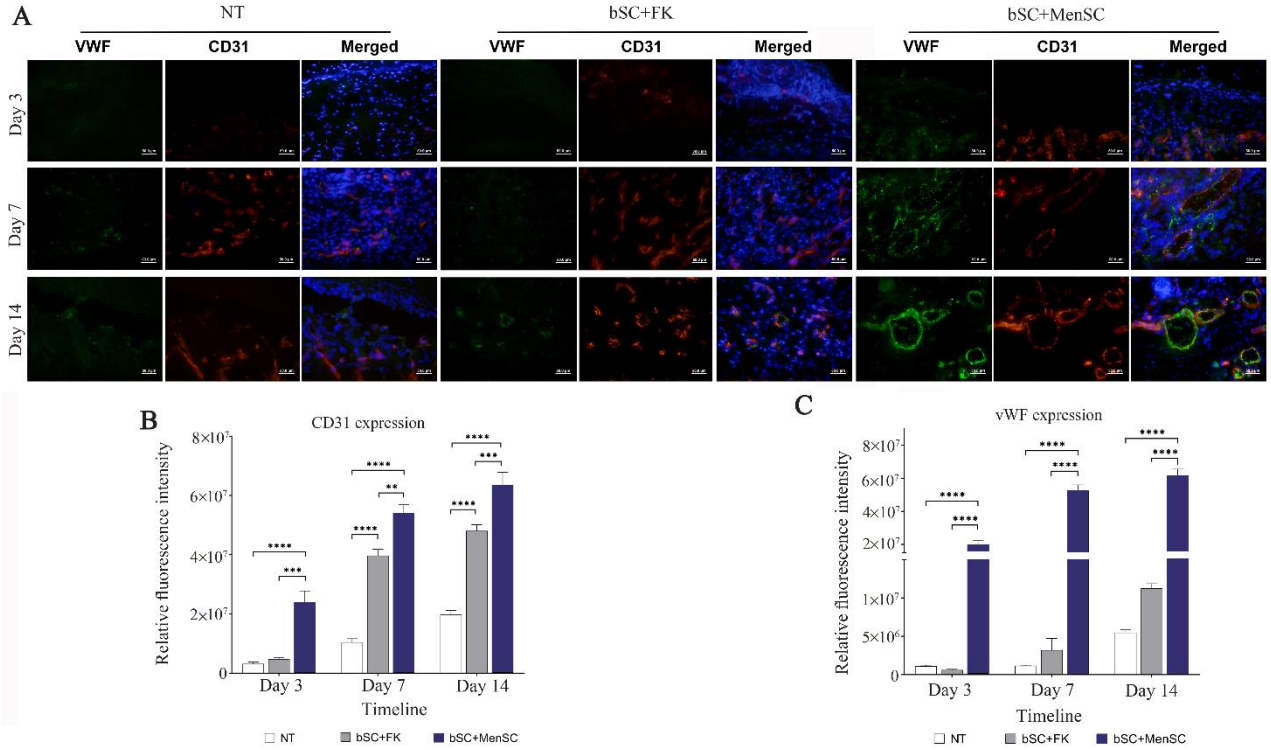

Figure 8. Angiogenesis and Vasculogenesis evaluations in diabetic wound healing. A) Diabetic wound sections were labeled by double immunofluorescence staining of CD31 and vWF expression pattern through PE conjugated anti-CD31 and Alexa Fluor®488 conjugated anti-vWF. These sections were also counterstained with DAPI. Scale bar = 50 μm. Comparative evaluation of relative fluorescence intensity of CD31 expression, B) and vWF expression, C) were evaluated on days 3, 7 and 14 in diabetic wounds. p-values less than 0.05, 0.01, 0.001, and 0.0001 were shown with *, **, ***, and ****, respectively.

that integrated into wound bed [37]. Interestingly, IVL expression was considerably higher in MenSCs seeded bilayer scaffold wound dressing in comparison with other groups at day 7 and day 14. In previous studies [38,39], we indicated that MenSCs could potentially differentiate into mature keratinocytes and express several epidermal specific markers such as K14, p63, and IVL. Collectively, it can be concluded that higher expression level of IVL in bSC+MenSCs group might be also considered as trans-differentiation of MenSC phenotype into keratinocytes in diabetic wound bed dressed by MenSCs-seeded bilayer scaffold. Moreover, dermal thickness in bSC+MenSCs group represented noteworthy increase during 7 days after wound induction in comparison to bSC+FK and NT groups. H&E examination confirmed increased DTI index in bSC+MenSCs group and decreasing dermal cellularity to normal level same as adjacent skin at day 14. However, dermal thickness in diabetic wound site in NT and bSC+FK groups were less than normal adjacent skin after 14 days, thus low proliferation rate and ECM deposition contribute to impaired wound healing. These results confirm that sustained inflammation in chronic wounds, lead to fibroblast dysfunction [40]. Hence, in line with our findings, seeded fibroblast/keratinocyte on bilayer scaffold wound dressing has not been as effective as MenSCs-seeded bilayer scaffold in progression of regenerative procedures in diabetic wounds.

In early phase of wound healing, deposition of ECM proteins particularly type III collagen happens in dermis [41,42] and consistent with our previous findings [20]. In early phase of wound healing, deposition of ECM proteins particularly type III collagen happens in dermis [41,42]. In consistent with our previous findings, contrary to upward trend of total collagen from day 3 to day 14 in other groups, MenSCs-seeded bilayer scaffold wound dressing inversely showed downward trend of type III from day 7 to day 14 [20]. Therefore, accumulation of type I collagen deposition has been proposed as a characteristic of newly formed dermis maturation [43]. Our data showed that maximum dermal hypertrophy and expression of type III collagen were observed in bSC+MenSCs group at day 7 and further at day 14 more than two-fold reduction was determined in type III collagen density. In line with these findings, it was reported that recruitment of MenSCs in normal wound healing in mice lead to deposition of well-organized collagen fibers in dense thick bundles following reduction of type III collagen proportion [31], as well as MMPs during remodeling phase. MMP-9 play a detrimental role in diabetic wound healing [44] and the evaluation of

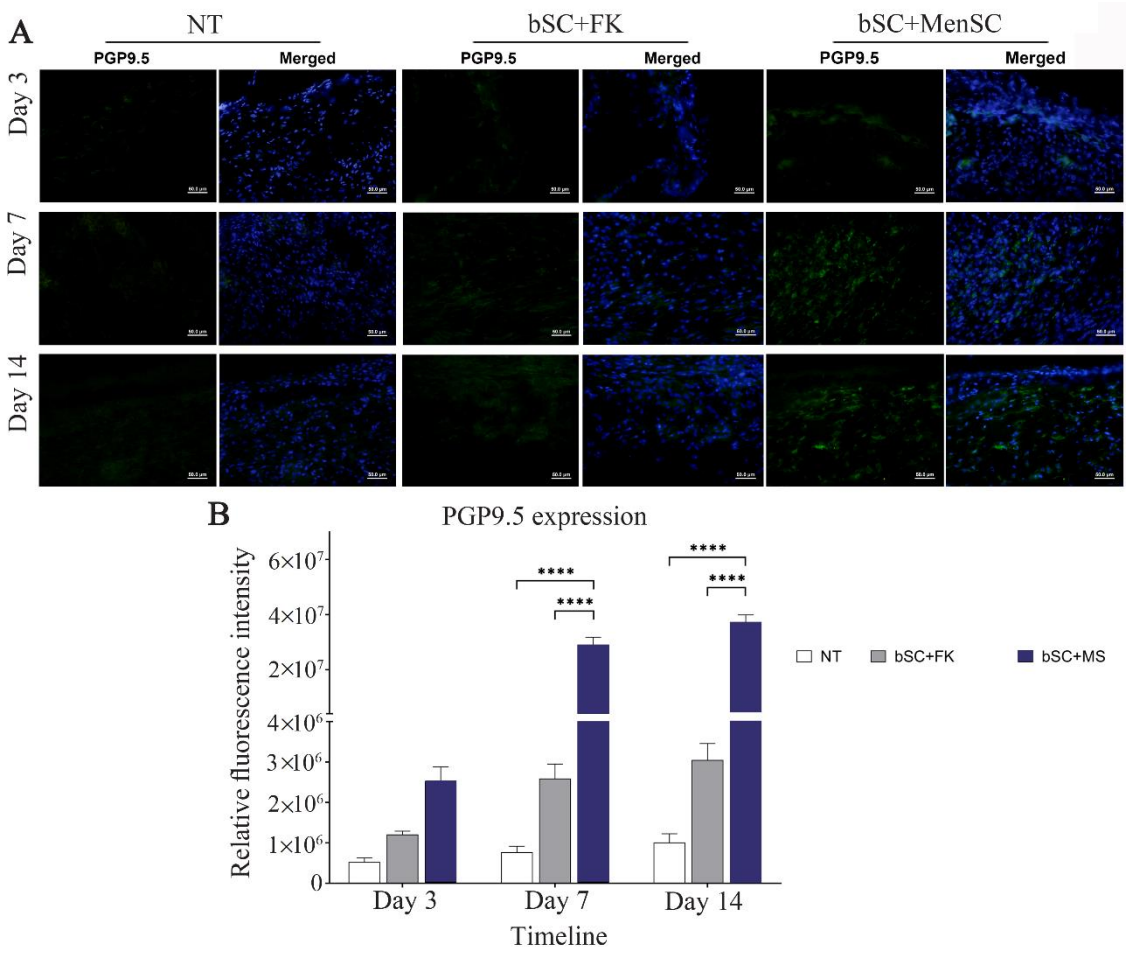

Figure 9. Evaluation of innervation pattern in diabetic wound healing. A) Diabetic wound sections were labeled by immunofluorescence staining of PGP9.5 expression pattern through Alexa Fluor®488 conjugated anti- PGP9.5. Indirect immunofluorescence staining for innervation assessment targeted diabetic wounds. These sections were also counterstained with DAPI. Scale bar = 50 μm. B) Comparative evaluation of relative fluorescence intensity of PGP9.5 expressions in diabetic wound. p-values less than 0.05, 0.01, 0.001, and 0.0001 were shown with *, **, ***, and ****, respectively.

MMP-9 expression can be an accurate prediction of the success in treatment of the chronic wound [45].

Consistent with previous data, our results exemplified by diabetic wound dressed by MenSCs seeded bilayer scaffold, the level of MMP-9 mRNA expression was significantly decreased from day 7 to day 14 in comparison to NT group and FK+bSC group. However, we observed that lower level of the MMP-9 mRNA along with fibroblast/keratinocyte-seeded bilayer scaffold wound dressing in comparison to no treated wounds at day 7 after diabetic wound induction, is likely to be related to the short-term role of fibroblasts implanted on bilayer scaffold in modulating inflammation through the secretion of protease inhibitors, including TIMP-1 and -2 [46-48].

In diabetic wound, it has been reported that inflamed wound chronicity and oxidative stress lead to premature senescence and irreversible arrest of proliferation in fibroblasts [49]. Furthermore, keratinocytes in the chronic wound are unable to upregulate chemokines and cytokines are necessary for the resolution of inflammation [50] and in diabetic wound due to prolonged inflammation phase, excessive infiltration of leukocytes lead to non-healing wound process [51-53]. Our data designated that the recruitment of fibroblast/keratinocyte-seeded bilayer scaffold could considerably reduce inflammation at day 3 and day 7 in comparison to NT group, but at day 14 according to prolonged inflammatory state and sustained inflammatory phase there were no significant differences in the amount of the neutrophils between bSC+FK and NT groups. On the other hand, the diabetic wound dressed by MenSCs-seeded bilayer scaffold showed a significantly downward trend of neutrophil accumulation in wound bed in comparison to NT group in all studied time points. Furthermore, bSC+MenSCs group showed the lowest numbers of neutrophils in comparison with bSC+FK and NT groups at day 14. Collectively, its seems that due to non-resolving chronic inflammation, keratinocytes and fibroblasts represented impaired abil-

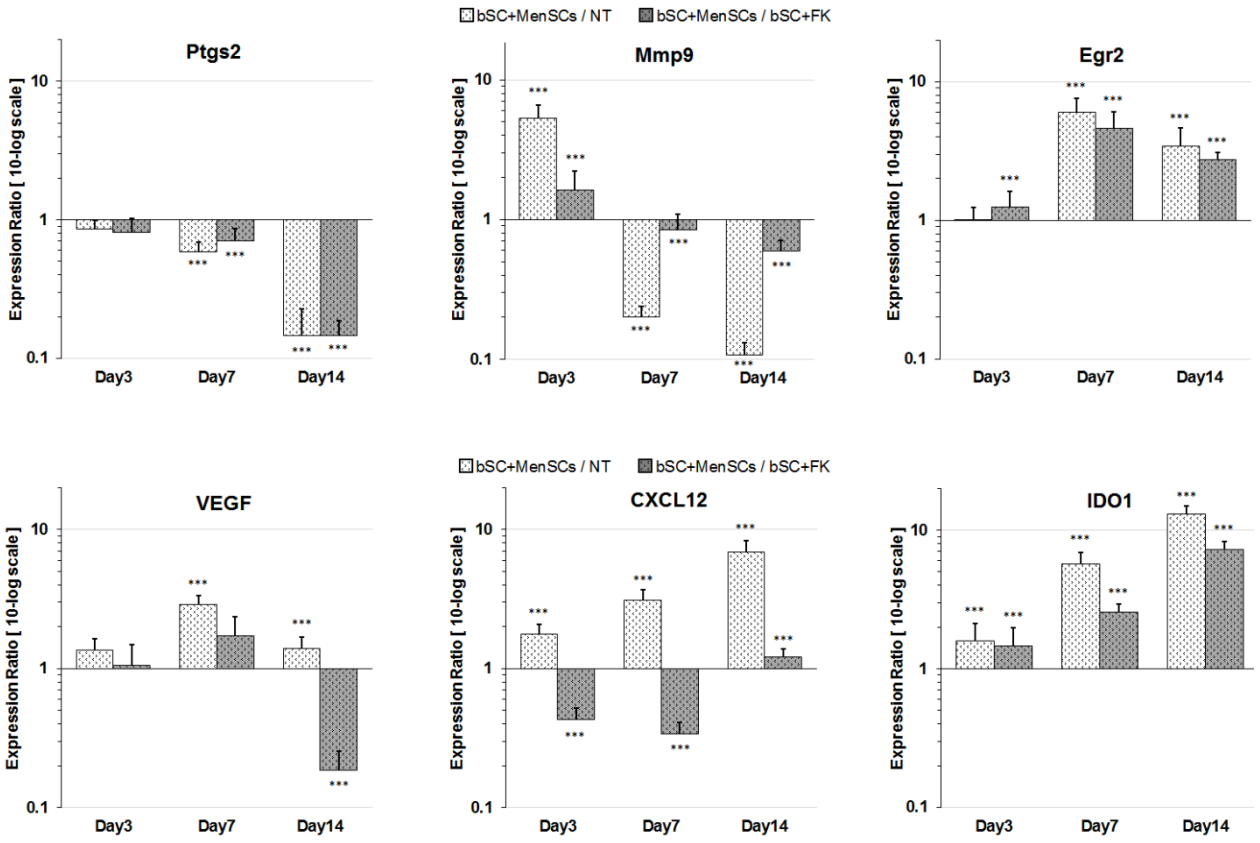

Figure 10. Relative gene expression ratio of some wound healing related genes by different wound dressing. Matrix early growth response 2 (Egr2), metallopeptidase 9 (Mmp9), chemokine (C-X-C motif) ligand 12 (CXCL12 or SDF-1), indoleamine 2,3-dioxygenase 1 (IDO1), prostaglandin-endoperoxide synthase 2 (Ptgs2), vascular endothelial growth factor A (VEGFA) in diabetic wound areas of mice. The expression is normalized to the reference gene (B2m). There were five cases in each group. p-values less than 0.05, 0.01, 0.001, and 0.0001 were shown with *, **, ***, and ****, respectively.

ity to upregulate anti-inflammatory cytokines and chemokines and this cell-based bioengineered wound substitute could not promote delayed wound healing [40,50].

In consistent with previous results, noticeable distribution of M1 macrophages was detected in the diabetic wound site in bSC+FK and NT groups during 14 days. However, the lowest number of M1 phenotype was noticed in diabetic wound dressed by MenSCs-seeded bilayer scaffold at day 14. Conversely, the greatest number of M2 phenotype presented in wounds treated with MenSCs-seeded bilayer scaffold at day 7 and day 14. In line with these findings, we determined significantly higher *Egr2* mRNA expression (the gene involved in M2 macrophage polarization) at day 7 and day 14 in bSC+MenSCs group in comparison to other groups. According to previous reports [40,54], prolonged inflammation in the chronic wound bed might lead to fibroblast dysfunction.

Furthermore, Galkowska *et al* found that keratinocytes and endothelial cells in the chronic wound site are unable to upregulate necessary chemokines and cytokines, and that in turn, continual elevation of Reactive Oxygen Species (ROS), might also occur [50]. Overproduction of ROS lead to ECM and cell membrane damage [55], activation of proteases including MMPs and serine proteases and inactivation of protease inhibitors that result in premature cell senescence [56-58]. In fact, we represented that fibroblast/keratinocyte-seeded bilayer scaffold wound dressing failed to resolve inflammation and wound resolution.

In line with these findings, we also analyzed differential *Ptgs2* mRNA expression among study groups, while significantly ascending trend of cyclooxygenase (COX)-2 expression (*Ptgs2*) was determined during 14 days in no treatment group and diabetic wound dressed by fibroblast/keratinocyte-seeded bilayer scaffold. In contrast, significantly descending trend of *Ptgst2* in diabetic wound dressed by MenSCs-seeded bilayer scaffold indicated a substantial immunomodulatory effect of MenSCs in combination with bilayer scaffold applied in the wound site. We also evaluated the *IDO1* mRNA expression to identify the immunomodulatory role of MenSCs-seeded bilayer scaffold recruited in diabetic wound [59,60]. We observed that *IDO1* expression in diabetic wound bed significantly up-regulated

in bSC+MenSCs group especially in comparison to bSC+FK group and NT group during 14 days after diabetic wound induction.

In diabetic wound healing, successful wound revascularization failed to progress [61]. The results exhibited that noteworthy increased expression of CD31 occurs in bSC+MenSCs group as well as in bSC+FK group in comparison to no treatment group at day 7 and day 14. Although, diabetic wounds dressed by MenSCs-seeded bilayer scaffold presented higher expression of CD31 even in comparison to bSC+FK group from day 7 to day 14. Interestingly, the strongest expression of vWF in diabetic wounds were identified when wounds were dressed by MenSCs-seeded bilayer scaffold at three time points. We also assessed *CXCL12* or *SDF-1* mRNA expression level in diabetic mice wounds as a principal chemokine involved in recruiting of Endothelial Precursor Cells (EPCs) into the wound site [62]. In agreement with immunofluorescence evaluation of CD31, the qRT-PCR analysis also showed significant expression of *CXCL12* mRNA in bSC+MenSCs group in comparison with no treated diabetic wounds. Hence, the immunomodulatory potency and specific paracrine effect of MenSCs in combination with bilayer scaffold properties resulted in reducing prolonged inflammation of diabetic wound and enhance angiogenesis and neovascularization [31,32,63] or even their differentiation into mature endothelial-like cells [33,34].

To our knowledge, polarization of macrophages from pro-inflammatory M1 phenotype into anti-inflammatory M2 phenotypes occur in the latter stages of wound healing [35,64]. M2 macrophages that represent pro-healing functions, play a critical role in epithelialization and innervation in wound healing through producing anti-inflammatory and pro-resolving neuroprotectin/protectin D1 (NPD1/PD1) [65]. Persistent chronic inflammation in diabetic wounds causes excessive or unresolved M1 macrophage activation which contributes to the impairment of wound healing and repairing of injured peripheral nerves, in turn results in diabetic peripheral neuropathy and pain insensitivity [66,67]. In this study, the up-regulation of *PGP9.5* was significantly observed in diabetic wound dressed by MenSCs-seeded bilayer scaffold in comparison to other groups at day 7 and day 14. Consistent with this data, it has been shown that macrophages produce anti-inflammatory and pro-resolving NPD1 involved in attenuating macrophage inflammatory activities, chronic inflammation and oxidative stress after unresolved inflammation in diabetic wound [65].

Collectively, our results indicate that MenSCs in conjunction with bilayer scaffold provide a specialized stem cell-derived skin substitute and exhibits a complex of immunomodulatory, clonogenicity, migratory and specific paracrine signature necessary to enhance regeneration in non-healing diabetic wound environment. Fibroblast/keratinocyte-seeded bilayer scaffold wound dressing was considered as a compensatory reparative population, however in diabetic wounds, collagen remodeling and ECM formation are prevented and fibroblasts and keratinocytes exhibit reduced reaction to growth factors, lower migratory ability, and increased apoptosis rate [40,68]. Also, inability of fibroblast and keratinocyte to express anti-inflammatory functions because of persistence of inflammatory state in diabetic wound microenvironment resulted in irreversible growth arrest or replicative senescence in quiescent fibroblasts settled in wound bed [40]. Consequently, senescent fibroblast probably could not contribute to mobilization of EPCs from bone marrow niches toward the wound site and homing to diabetic wound bed [69]. In fact, chronic inflammation [70,71] and bacterial infection [72,73] play contributory roles in scar formation and insufficient regeneration in diabetic wound bed and fail to obtain satisfactory results [74,75].

Conclusion

This study shows that MenSCs with their superior biological properties, including potent immunomodulatory, proangiogenic and reparative potential in combination with bioengineered bilayer scaffold skin substitute not only enhanced diabetic wound healing and cutaneous regeneration process *in vivo*, but also may be relevant for the clinical application and treatment of diabetic impaired wound healing process. From the current study, it seems that fibroblast and keratinocyte cells-loaded bilayer scaffold like commercial cell-based skin substitutes are unable to attenuate pro-inflammatory microenvironment in diabetic mice model and promote impaired wound healing process. Future research should be conducted to explore the specific mechanisms involved in the enhanced immunomodulatory and reparative properties of MenSCs on chronic wound healing process.

References

1. Hart T, Milner R, Cifu A. Management of a diabetic foot. JAMA 2017;318(14):1387-8.
2. Akingboye AA, Giddins S, Gamston P, Tucker A, Navsaria H, Kyriakides C. Application of autologous derived-platelet rich plasma gel in the treatment of chronic wound ulcer: diabetic foot ulcer. J Extra Corpor Technol 2010;42(1):20-9.
3. Greaves NS, Iqbal SA, Baguneid M, Bayat A. The role of skin substitutes in the management of chronic cutaneous wounds. Wound Repair Regen 2013;21(2):194-210.
4. Farage MA, Miller KW, Berardesca E, Maibach HI. Psychological and social implications of aging skin: normal aging and the effects of cutaneous disease. Textbook of Aging Skin: Springer Berlin Heidelberg; 2010. p. 949-57.
5. Fisher GJ, Varani J, Voorhees JJ. Looking older: fibroblast collapse and therapeutic implications. Arch Dermatol 2008;144(5):666-72.
6. Rieger S, Zhao H, Martin P, Abe K, Lisse TS. The role of nuclear hormone receptors in cutaneous wound repair. Cell Biochem Funct 2015;33(1):1-13.

7. Sawicki G, Marcoux Y, Sarkhosh K, Tredget EE, Ghahary A. Interaction of keratinocytes and fibroblasts modulates the expression of matrix metalloproteinases-2 and-9 and their inhibitors. Mol Cell Biochem 2005;269 (1):209-16.
8. Gill SE, Parks WC. Metalloproteinases and their inhibitors: regulators of wound healing. Int J Biochem Cell Biol 2008;40(6-7):1334-47.
9. Werner S, Krieg T, Smola H. Keratinocyte–fibroblast interactions in wound healing. J Invest Dermatol 2007; 127(5):998-1008.
10. de Mulder EL, Hannink G, van Kuppevelt TH, Daamen WF, Buma P. Similar hyaline-like cartilage repair of osteochondral defects in rabbits using isotropic and anisotropic collagen scaffolds. Tissue Eng Part A 2014; 20(3-4):635-45.
11. Dulauroy S, Di Carlo SE, Langa F, Eberl G, Peduto L. Lineage tracing and genetic ablation of ADAM12+ perivascular cells identify a major source of profibrotic cells during acute tissue injury. Nat Med 2012;18(8): 1262-70.
12. Labarrere CA, Woods J, Hardin J, Campana G, Ortiz M, Jaeger B, et al. Early prediction of cardiac allograft vasculopathy and heart transplant failure. Am J Transplant 2011;11(3):528-35.
13. Lemos DR, Duffield JS. Tissue-resident mesenchymal stromal cells: Implications for tissue-specific antifibrotic therapies. Sci Transl Med 2018;10(426):eaan5174.
14. Vander Beken S, de Vries JC, Meier-Schiesser B, Meyer P, Jiang D, Sindrilaru A, et al. Newly defined ATP-binding cassette subfamily B member 5 positive dermal mesenchymal stem cells promote healing of chronic iron-overload wounds via secretion of interleukin-1 receptor antagonist. Stem Cells 2019;37(8): 1057-74.
15. Finch PW, Rubin JS, Miki T, Ron D, Aaronson SA. Human KGF is FGF-related with properties of a paracrine effector of epithelial cell growth. Science 1989; 245(4919):752-5.
16. Rubin JS, Osada H, Finch PW, Taylor WG, Rudikoff S, Aaronson SA. Purification and characterization of a newly identified growth factor specific for epithelial cells. Proc Natl Acad Sci USA 1989;86(3):802-6.
17. Martin P, Parkhurst SM. Parallels between tissue repair and embryo morphogenesis. Development 2004 Jul;131 (13):3021-34.
18. Arasteh S, Kazemnejad S, Khanjani S, Heidari-Vala H, Akhondi MM, Mobini S. Fabrication and characterization of nano-fibrous bilayer composite for skin regeneration application. Methods 2016;99:3-12.
19. Arasteh S, Khanjani S, Golshahi H, Mobini S, Jahed MT, Heidari-Vala H, et al. Efficient wound healing using a synthetic nanofibrous bilayer skin substitute in murine model. J Surg Res 2020;245:31-44.
20. Mirzadegan E, Golshahi H, Saffarian Z, Darzi M, Khorasani S, Edalatkhah H, et al. The remarkable effect of menstrual blood stem cells seeded on bilayer scaffold composed of amniotic membrane and silk fibroin aiming to promote wound healing in diabetic mice. Int Immunopharmacol 2021:108404.
21. Jung JA, Yoon YD, Lee HW, Kang SR, Han SK. Comparison of human umbilical cord blood-derived mesenchymal stem cells with healthy fibroblasts on wound-healing activity of diabetic fibroblasts. Int Wound J 2018;15(1):133-9.
22. O'Loughlin A, Kulkarni M, Creane M, Vaughan EE, Mooney E, Shaw G, et al. Topical administration of allogeneic mesenchymal stromal cells seeded in a collagen scaffold augments wound healing and increases angiogenesis in the diabetic rabbit ulcer. Diabetes 2013; 62(7):2588-94.
23. Kuo Y-R, Wang C-T, Cheng J-T, Wang F-S, Chiang Y-C, Wang C-J. Bone marrow–derived mesenchymal stem cells enhanced diabetic wound healing through recruitment of tissue regeneration in a rat model of streptozotocin-induced diabetes. Plast Reconstr Surg 2011;128 (4):872-80.
24. de Mayo T, Conget P, Becerra-Bayona S, Sossa CL, Galvis V, Arango-Rodríguez ML. The role of bone marrow mesenchymal stromal cell derivatives in skin wound healing in diabetic mice. PLoS One 2017;12(6): e0177533.
25. Garber JC, Wayne Barbee R, Bielitzki JT, Clayton LA, Donovan JC, Hendriksen C, et al. Committee for the Update of the Guide for the Care and Use of Laboratory Animals. Guide for the Care and Use of Laboratory Animals, eighth ed Washington DC, USA: National Academy of Sciences. 2011.
26. Fathi-Kazerooni M, Kazemnejad S, Khanjani S, Saltanatpour Z, Tavoosidana G. Down-regulation of mir-122 after transplantation of mesenchymal stem cells in acute liver failure in mice model. Biologicals 2019;58: 64-72.
27. Zare S, Zarei MA, Ghadimi T, Fathi F, Jalili A, Hakhamaneshi MS. Isolation, cultivation and transfection of human keratinocytes. Cell Biol Int 2014;38(4):444-51.
28. Mujaj S, Manton K, Upton Z, Richards S. Serum-free primary human fibroblast and keratinocyte coculture. Tissue Eng Part A 2010;16(4):1407-20.
29. Flanagan M. Wound measurement: can it help us to monitor progression to healing? J Wound Care 2003; 12(5):189-94.
30. Alcayaga-Miranda F, Cuenca J, Luz-Crawford P, Aguila-Díaz C, Fernandez A, Figueroa FE, et al. Characterization of menstrual stem cells: angiogenic effect, migration and hematopoietic stem cell support in comparison with bone marrow mesenchymal stem cells. Stem Cell Res Ther 2015;6(1):1-14.
31. Cuenca J, Le-Gatt A, Castillo V, Belletti J, Díaz M, Kurte G, et al. The reparative abilities of menstrual stem cells modulate the wound matrix signals and improve cutaneous regeneration. Front Physiol 2018;9:464.
32. Ulrich D, Edwards SL, Su K, Tan KS, White JF, Ramshaw JA, et al. Human endometrial mesenchymal stem cells modulate the tissue response and mechanical behavior of polyamide mesh implants for pelvic organ prolapse repair. Tissue Eng Part A 2014;20(3-4):785-98.
33. Zografou A, Papadopoulos O, Tsigris C, Kavantzas N, Michalopoulos E, Chatzistamatiou T, et al. Autologous

transplantation of adipose-derived stem cells enhances skin graft survival and wound healing in diabetic rats. Ann Plast Surg 2013;71(2):225-32.

34. Oswald J, Boxberger S, Jørgensen B, Feldmann S, Ehninger G, Bornhäuser M, et al. Mesenchymal stem cells can be differentiated into endothelial cells in vitro. Stem Cells 2004;22(3):377-84.
35. Jablonski KA, Amici SA, Webb LM, Ruiz-Rosado JdD, Popovich PG, Partida-Sanchez S, et al. Novel markers to delineate murine M1 and M2 macrophages. PLoS One 2015;10(12):e0145342.
36. Livak KJ, Schmittgen TD. Analysis of relative gene expression data using real-time quantitative PCR and the 2− ΔΔCT method. Methods 2001;25(4):402-8.
37. Ghahary A, Ghaffari A. Role of keratinocyte–fibroblast cross-talk in development of hypertrophic scar. Wound Repair Regen 2007;15:S46-S53.
38. Akhavan-Tavakoli M, Fard M, Khanjani S, Zare S, Edalatkhah H, Mehrabani D, et al. In vitro differentiation of menstrual blood stem cells into keratinocytes: A potential approach for management of wound healing. Biologicals 2017;48:66-73.
39. Fard M, Akhavan-Tavakoli M, Khanjani S, Zare S, Edalatkhah H, Arasteh S, et al. Bilayer amniotic membrane/nano-fibrous fibroin scaffold promotes differentiation capability of menstrual blood stem cells into keratinocyte-like cells. Mol Biotechnol 2018;60(2):100-10.
40. Wall IB, Moseley R, Baird DM, Kipling D, Giles P, Laffafian I, et al. Fibroblast dysfunction is a key factor in the non-healing of chronic venous leg ulcers. J Invest Dermatol 2008;128(10):2526-40.
41. Weinzweig J. Plastic Surgery Secrets Plus E-Book: Elsevier Health Sciences; 2010.
42. Tracy LE, Minasian RA, Caterson E. Extracellular matrix and dermal fibroblast function in the healing wound. Adv Wound Care (New Rochelle) 2016;5(3):119-36.
43. Han G, Nguyen LN, Macherla C, Chi Y, Friedman JM, Nosanchuk JD, et al. Nitric oxide–releasing nanoparticles accelerate wound healing by promoting fibroblast migration and collagen deposition. Am J Pathol 2012;180(4):1465-73.
44. Nguyen TT, Ding D, Wolter WR, Pérez RL, Champion MM, Mahasenan KV, et al. Validation of matrix metalloproteinase-9 (MMP-9) as a novel target for treatment of diabetic foot ulcers in humans and discovery of a potent and selective small-molecule MMP-9 inhibitor that accelerates healing. J Med Chem 2018;61(19):8825-37.
45. Xu J, Zgheib C, Hodges MM, Caskey RC, Hu J, Liechty KW. Mesenchymal stem cells correct impaired diabetic wound healing by decreasing ECM proteolysis. Physiol Genomics 2017;49(10):541-8.
46. Kut-Lasserre C, Miller CC, Ejeil A, Gogly B, Dridi M, Piccardi N, et al. Effect of avocado and soybean unsaponifiables on gelatinase A (MMP-2), stromelysin 1 (MMP-3), and tissue inhibitors of matrix metalloproteinase (TIMP-1 and TIMP-2) secretion by human fibroblasts in culture. J Periodontol 2001;72(12):1685-94.
47. Ravanti L, Kähäri V-M. Matrix metalloproteinases in wound repair. Int J Mol Med 2000;6(4):391-798.
48. Tandara AA, Mustoe TA. MMP-and TIMP-secretion by human cutaneous keratinocytes and fibroblasts–impact of coculture and hydration. J Plast Reconstr Aesthet Surg 2011;64(1):108-16.
49. Wlaschek M, Scharffetter-Kochanek K. Oxidative stress in chronic venous leg ulcers. Wound Repair Regen 2005;13(5):452-61.
50. Galkowska H, Wojewodzka U, Olszewski WL. Chemokines, cytokines, and growth factors in keratinocytes and dermal endothelial cells in the margin of chronic diabetic foot ulcers. Wound Repair Regen 2006;14(5):558-65.
51. Wilgus TA, Roy S, McDaniel JC. Neutrophils and wound repair: positive actions and negative reactions. Adv Wound Care (New Rochelle) 2013;2(7):379-88.
52. Loots MA, Lamme EN, Zeegelaar J, Mekkes JR, Bos JD, Middelkoop E. Differences in cellular infiltrate and extracellular matrix of chronic diabetic and venous ulcers versus acute wounds. J Invest Dermatol 1998;111(5):850-7.
53. Larouche J, Sheoran S, Maruyama K, Martino MM. Immune regulation of skin wound healing: mechanisms and novel therapeutic targets. Adv Wound Care (New Rochelle) 2018;7(7):209–31.
54. Dimri GP, Lee X, Basile G, Acosta M, Scott G, Roskelley C, et al. A biomarker that identifies senescent human cells in culture and in aging skin in vivo. Proc Natl Acad Sci USA 1995;92(20):9363-7.
55. Ben-Porath I, Weinberg RA. The signals and pathways activating cellular senescence. T Int J Biochem Cell Biol 2005;37(5):961-76.
56. Wysocki AB, Staiano-Coico L, Grinnell F. Wound fluid from chronic leg ulcers contains elevated levels of metalloproteinases MMP-2 and MMP-9. J Invest Dermatol 1993;101(1):64-8.
57. Weckroth M, Vaheri A, Lauharanta J, Sorsa T, Konttinen YT. Matrix metalloproteinases, gelatinase and collagenase, in chronic leg ulcers. J Invest Dermatol 1996;106(5):1119-24.
58. Saarialho-Kere U. Patterns of matrix metalloproteinase and TIMP expression in chronic ulcers. Arch Dermatol Res 1998;290(1):S47-S54.
59. Krampera M, Cosmi L, Angeli R, Pasini A, Liotta F, Andreini A, et al. Role for interferon-γ in the immunomodulatory activity of human bone marrow mesenchymal stem cells. Stem Cells 2006;24(2):386-98.
60. Shokri M-R, Bozorgmehr M, Ghanavatinejad A, Falak R, Aleahmad M, Kazemnejad S, et al. Human menstrual blood-derived stromal/stem cells modulate functional features of natural killer cells. Sci Rep 2019;9(1):1-13.
61. Nuschke A. Activity of mesenchymal stem cells in therapies for chronic skin wound healing. Organogenesis 2014;10(1):29-37.
62. Ceradini DJ, Kulkarni AR, Callaghan MJ, Tepper OM, Bastidas N, Kleinman ME, et al. Progenitor cell trafficking is regulated by hypoxic gradients through HIF-1 induction of SDF-1. Nat Med 2004;10(8):858-64.

63. Alcayaga-Miranda F, Cuenca J, Luz-Crawford P, Aguila-Díaz C, Fernandez A, Figueroa FE, et al. Characterization of menstrual stem cells: angiogenic effect, migration and hematopoietic stem cell support in comparison with bone marrow mesenchymal stem cells. Stem Cell Res Ther 2015;6(1):32.

64. Hesketh M, Sahin KB, West ZE, Murray RZ. Macrophage phenotypes regulate scar formation and chronic wound healing. Int J Mol Sci 2017;18(7):1545.

65. Hong S, Tian H, Lu Y, Laborde JM, Muhale FA, Wang Q, et al. Neuroprotectin/protectin D1: endogenous biosynthesis and actions on diabetic macrophages in promoting wound healing and innervation impaired by diabetes. Am J Physiol Cell Physiol 2014;307(11): C1058-C67.

66. Dinh TL, Veves A. A review of the mechanisms implicated in the pathogenesis of the diabetic foot. Int J Low Extrem Wounds 2005;4(3):154-9.

67. Schwab JM, Chiang N, Arita M, Serhan CN. Resolvin E1 and protectin D1 activate inflammation-resolution programmes. Nature 2007;447(7146):869-74.

68. Loots MA, Lamme EN, Mekkes JR, Bos JD, Middelkoop E. Cultured fibroblasts from chronic diabetic wounds on the lower extremity (non-insulin-dependent diabetes mellitus) show disturbed proliferation. Arch Dermatol Res 1999;291(2-3):93-9.

69. Parsonage G, Filer AD, Haworth O, Nash GB, Rainger GE, Salmon M, et al. A stromal address code defined by fibroblasts. Trends Immunol 2005;26(3):150-6.

70. Agren M, Eaglstein WH, Ferguson M, Harding KG, Moore K, Saarialho-Kere U, et al. Causes and effects of the chronic inflammation in venous leg ulcers. Acta Derm Venereol Suppl (Stockh) 2000;210:3-17.

71. Coleridge Smith PD. Update on chronic-venous-insufficiency-induced inflammatory processes. Angiology 2001;52(1_suppl):S35-S42.

72. Robson MC. Wound infection: a failure of wound healing caused by an imbalance of bacteria. Surg Clin North Am 1997;77(3):637-50.

73. Dow G, Browne A, Sibbald R. Infection in chronic wounds: controversies in diagnosis and treatment. Ostomy Wound Manage 1999;45(8):23-7, 29-40.

74. Brem H, Stojadinovic O, Diegelmann RF, Entero H, Lee B, Pastar I, et al. Molecular markers in patients with chronic wounds to guide surgical debridement. Mol Med 2007;13(1-2):30-9.

75. Stojadinovic O, Brem H, Vouthounis C, Lee B, Fallon J, Stallcup M, et al. Molecular pathogenesis of chronic wounds: the role of β-catenin and c-myc in the inhibition of epithelialization and wound healing. Am J Pathol 2005;167(1):59-69.